Changes in weak pair-wise correlations during running reshapes network state in the main olfactory bulb

Udaysankar Chockanathan [1,2,+], Emily J. W. Crosier[2,+], Spencer Waddle [3], Edward Lyman[3], Richard C. Gerkin [4], Krishnan Padmanabhan[1,2,5,] *

1. Medical Scientist Training Program
2. Department of Neuroscience and Neuroscience Graduate Program (NGP) University of Rochester School of Medicine, Rochester, NY 14642
3. Department of Physics, University of Delaware, Newark, DE 19716
4. School of Life Sciences, Arizona State University, Tempe, AZ 85287
5. Center for Visual Sciences, University of Rochester School of Medicine, Rochester, NY 14620

+. These authors contributed equally to the work

* correspondence: Krishnan_padmanabhan@urmc.rochester.edu

Abstract

Neural codes for sensory representations are thought to reside in a broader space defined by the patterns of spontaneous activity that occur when stimuli are not being presented. To understand the structure of this spontaneous activity in the olfactory system, we performed high-density recordings of population activity in the main olfactory bulb of awake mice. We found that spontaneous activity patterns of ensembles of mitral and tufted (M/T) cells in the main olfactory bulb changed dramatically during locomotion, including decreases in pairwise correlations between neurons and increases in the entropy of the population. Maximum entropy models of the ensemble activity revealed that pair-wise interactions were better at predicting patterns of activity when the animal was stationary than while running, suggesting that higher order (3rd, 4th order) interactions between neurons shape activity during locomotion. Taken together, we found that locomotion influenced the structure of spontaneous population activity at the earliest stages of olfactory processing, 1 synapse away from the sensory receptors in the nasal epithelium.

36 **New and Noteworthy**

37 The organization and structure of spontaneous population activity in the olfactory
38 system places constraints of how odor information is represented. Using high-density
39 electrophysiological recordings of mitral and tufted cells, we found that running
40 increases the dimensionality of spontaneous activity, implicating higher-order
41 interactions among neurons during locomotion. Behavior thus flexibly alters neuronal
42 activity at the earliest stages of sensory processing.

43

Introduction

Behavioral states, such as quiescence and wakefulness (Constantinople and Bruno 2011), locomotion (Dadarlat and Stryker 2017; Dipoppa et al. 2018) and arousal (Vinck et al. 2015) can have marked effects on patterns of neuronal activity throughout the brain. In sensory systems, neural activity can change in response to these behaviors, absent any sensory stimuli. This spontaneous activity often reflects the underlying organization of the circuit (Niell and Stryker 2010; Tsodyks et al. 1999), constraining what types of activity patterns are possible for encoding sensory stimuli (Luczak et al. 2009). These latent behavioral states consequently shape the variability of neuronal responses in primary sensory areas (Stringer et al. 2019)

As in the neocortex, neural activity in the main olfactory bulb is strongly influenced by behavioral state (Tsuno and Mori 2009). The principal neurons of the main olfactory bulb, the mitral and tufted cells (M/T) which receive direct input from the olfactory receptor neurons (ORNs), process these initial odor representations via connections with one another and with local inhibitory interneurons, and relay this information to downstream cortical areas (Wilson and Mainen 2006). Spontaneous firing rates in the principal M/T are lower under anesthesia as compared to waking (Rinberg et al. 2006a) and their activity can indicate non-olfactory information such as behavioral choice (Doucette and Restrepo 2008; Kay and Laurent 1999) or reward (Doucette et al. 2011). M/T cell firing can also be altered based on experience and training (Abraham et al. 2010; Kobayakawa et al. 2007; Smear et al. 2013). While the behavioral modulation of M/T activity is not surprising, given the link between olfaction, sniffing, and whisking (Carey and Wachowiak 2011; Kleinfeld et al. 2014; Moore et al.

2013; Verhagen et al. 2007), the fact that it occurs in principal cells one synapse away from the sensory periphery (Murthy 2011; Wilson and Mainen 2006) suggests that the impact of behavior on neuronal coding may occur earlier in olfactory processing (Tsuno et al. 2008) as compared to other sensory systems in mammals. Centrifugal projections into the bulb (Padmanabhan et al. 2016; Price and Powell 1970, 1971; Shipley and Adamek 1984) from a diversity of areas including in the hippocampus (Davis and Macrides 1981; Padmanabhan et al. 2018), point to a density of anatomical connections that link olfactory processing in the bulb to a complex array of behaviors (Gourevitch et al. 2010) including running. While a number of recent studies suggest that locomotion and running exert substantial influence on population activity in sensory neocortices (Dadarlat and Stryker 2017; Dipoppa et al. 2018; Erisken et al. 2014; Stringer et al. 2019), it is less clear how locomotion, which is essential for a number of olfactory behaviors including foraging (Gire et al. 2016), and tracking (Khan et al. 2012), influences the activity of ensembles of neurons in the earliest stages of olfactory coding.

To address this, we recorded simultaneously from 100s of M/T cells in main olfactory bulb (MOB) while animals ran on a cylindrical wheel. Not only did running increase firing rates in individual neurons, running also change the structure of activity across populations of cells, including increased the entropy of the ensemble activity. An Ising maximum entropy model of M/T cell firing patterns uncovered that small changes in the pair-wise interactions between neurons during locomotion had large effects on the global structure of population activity when the animal was running. During locomotion, decreases in pair-wise interactions reduced the predictive power of 2nd order maxent

models, opening up the possibility that higher order structure in the shapes neural population activity.

Materials and Methods

Animals

All protocols and procedures were approved by the University Committee on Animal Resources (UCAR) at the University of Rochester and were performed in accordance with the guidelines of the Institutional Animal Care and Use Committee (IACUC) at the University of Rochester. 3 female and 2 male C57Bl6/J mice, age 3-6 months, were used in this study.

Surgery

Mice were anesthetized with an inhaled 1-2% isoflurane mixture. The scalp was removed and a 3D printed headframe was attached to the dorsal skull surface with veterinary adhesive (Vetbond, The 3M Company, Maplewood, MN, USA) and dental cement (Ortho-Jet Powder and Jet Liquid, Lang Dental Mfg. Co., Wheeling, IL, USA). A metal ground screw was also implanted into the skull. Following surgery, mice were monitored until they recovered from anesthesia. Post-operative analgesia was provided in accordance with approved protocols and animal weight was monitored during the week.

Run-wheel training

For a 5-day period following headframe implantation, mice were placed on a non-motorized running wheel for 1 hour daily. During these sessions, electrophysiological recordings were not performed. The purpose of these sessions was to acclimate the mice to running on a wheel while head-fixed. We previously found that following 5-days of exposure, both male and female mice habituate to the run wheel based on their running behavior, after which electrophysiology was performed (Warner and Padmanabhan 2020).

Electrophysiology

Mice were anesthetized with 1-2% inhaled isoflurane and a craniotomy was performed over the right main olfactory bulb using stereotactic coordinates (5 mm Rostral, 1 mm lateral, and 1-1.5 mm ventral of bregma). Immediately following the craniotomy, mice were transferred to the running wheel, where they were head-fixed and allowed to recover from anesthesia. A 128-channel nanofabricated silicon electrode array (Du et al. 2011) was vertically lowered into the MOB (**Fig. 1A,B**). Extracellular voltage recordings were collected at 30kHz in the 0.1-3500Hz frequency band (**Fig. 1C**). For four of the mice, one recording session was performed. For one mouse, a second recording session in a different region of the MOB was performed. Simultaneously, the running velocity of the mouse was also recorded via a rotational encoder attached to the wheel. All recordings were performed while mice were awake and behaving on the non-motorized voluntary running wheel. The recording rig was enclosed in a box to minimize interference from ambient odor, light, sound, and electromagnetic noise.

Spike sorting

Spike sorting was performed as previously described (Chockanathan et. al. 2020). Briefly, putative action potentials, or spikes, were identified as intervals during which the band-passed (500-3500 Hz) voltage magnitude exceeded 6 standard deviations from baseline. Periods containing voltage artifacts were manually identified and eliminated.

Spikes were assigned to units, or putative single neurons, by concatenating all the spikes on a channel with the signal from 8 neighboring channels and projecting them onto a space of principal components (PC) that explained 80% of the variance. Clusters were identified automatically using a mixture of Gaussians model (Lewicki 1998) and final manual curation was performed using criterion including the number of total spikes for that unit (>50), mean waveform shape, spike autocorrelogram, interspike interval, and waveform similarity across units .

Running behavior analysis

The motion of the run-wheel was controlled by the mouse, which could ambulate in forward or reverse directions or remain stationary. Wheel movement was converted to a velocity by integrating with a 150ms time bin in 10ms steps. Bins in which the velocity exceeded 1cm/s were classified as running and all other bins were classified as stationary.

Correlations

A sliding window was applied to the spike rasters to convert the binary spike pattern to a continuous firing rate trace, which was then converted to a z-score. The correlation coefficient between the running velocity and the activity of every unit in each animal was calculated. Null distributions of correlations were calculated by temporally shuffling spike times and generating instantaneous firing rate time-series from the shuffled spike trains.

Entropy

The spike train of each unit was binarized using 10ms non-overlapping bins. If one or more spikes from a given unit was present in a bin, the bin was assigned a value of 1. If no spikes were present in that bin, it was assigned a value of 0. This resulted in a binary matrix, in which each column describes the state of every neuron in the recorded population at a given time (Pryluk et al. 2019; de Ruyter van Steveninck et al. 1997; Schneidman et al. 2006). The probability distribution of these population states (entropy) was calculated as:

$$H = \sum_i -p_i \log_2 p_i \tag{1}$$

where H is the entropy and p_i is the probability of the ith pattern. For entropy analyses, the overall recorded population of neurons from each animal was subsampled 500 times. The number of neurons included in the subsample was varied between n = 3 neurons and 25 neurons. Entropy for running and stationary epochs was conditioned on the run velocity being greater than 1cm/sec

$$H_{stationary} = \sum_{i=1}^{N} -(p_i|stationary) \log_2 (p_i|stationary) \tag{2}$$

$$H_{running} = \sum_{i=1}^{N} -(p_i|running) \log_2 (p_i|running) \tag{3}$$

Maximum entropy models

The *maxent_toolbox* software (Maoz and Schneidman 2017) was used to fit the maximum entropy models (Ohiorhenuan et al. 2010; Schneidman et al. 2006). First, the local field terms h_i and pairwise interaction terms J_{ij} were computed from the binned spike trains. The resulting model was then used to predict the probability of each pattern:

$$P(\sigma_1, \sigma_2 \dots \sigma_N) = \frac{1}{Z} e^{\sum_i h_i \sigma_i + \frac{1}{2} \sum_{i \neq j} J_{ij} \sigma_i \sigma_j} \quad (4)$$

where σ_i denotes the binary state of each neuron and Z denotes the partition function, which normalizes the pattern probability distribution. The pattern probabilities predicted by the model were then compared to those observed in the data using the Kullback-Liebler divergence (KLD). The data binarization process used for the maximum entropy models is the same as that used for the entropy calculations.

Results

To study the effect of locomotion on spontaneous neuronal population activity, high-density 128 channel arrays were targeted to the MOB in head-fixed C57Bl6/J mice (n = 3 females, 2 males, age 3-6 months) trained to run on a non-motorized wheel (**Fig. 1A,B**). Action potentials in the extracellular recordings (**Fig. 1C**) were identified, and single-unit activity was clustered using a mixture-of-Gaussian models (Lewicki 1998) (**Fig. 1D-E**). Representative mean waveforms from putative M/T cells across all the channels in the electrode shank (**Fig. 1E**) illustrate the waveform diversity of units, with inter-spike interval (ISI) distributions (**Fig. 1F**) and autocorrelation functions (**Fig. 1G**)

202 reflecting the quality of spike-sorting (see methods). On average, 113 ± 46 well-isolated
203 units were identified per recording session (**Fig. 2A**).
204 Throughout the recordings, intervals of when the mouse remained stationary
205 were interspersed with epochs of running (inter-run interval as defined as the epoch
206 between the end of one run interval and the beginning of another = 6.2 ± 25.6s, **Fig.**
207 **2B**). In all animals, neuronal activity was dynamic both across and within stationary and
208 running epochs (**Fig. 2A**). At the single-animal level, mean firing rates during running
209 were significantly larger than those during stationary epochs in three animals
210 (Bonferroni-corrected $p < 0.05$, two-sided Wilcoxon signed-rank test, **Fig. 2C**). At the
211 group level, overall firing rates were increased with running ($FR_{stationary}$ = 1.86 ± 1.06Hz,
212 $FR_{running}$ = 2.10 ± 1.15Hz, $p < 0.05$, two-sided Wilcoxon signed-rank test, N = 6, **Fig.**
213 **2D**). Although average firing rates across the population increased with running,
214 individual neurons exhibited diverse changes in their activity patterns including both
215 increases and decreases in firing during locomotion. For example, a plot of the run
216 velocity of the animal and the firing rates for three example M/T cells showed units that
217 were negatively correlated, uncorrelated, or positively correlated with running velocity
218 (**Fig. 2E**). The range of correlations observed was significantly different than chance, as
219 determined using temporally shuffled spike trains ($p < 10^{-6}$, two-sample F-test, **Fig. 2F**).
220 As odor-encoding in the bulb is done not by single units, but relies on the activity
221 of ensembles of mitral and tufted cells from both the same (Dhawale et al. 2010) and
222 different glomeruli (Gerkin et al. 2013), we wished to examine how locomotion sculpted
223 the *collective* activity of neuronal populations in the MOB. First we visualized the
224 population activity of M/T ensembles in a low dimensional space defined by the first

three principle components calculated from the covariance of firing patterns across the entire recording duration for two example animals (**Fig. 3A1-2**). In these low-dimensional embeddings, ensemble activity when the animal was running was differentially distributed as compared to periods when the animal was stationary (**Fig. 3B1-2**). As a result, not only the structure of single neurons, but the activity of populations of cells was different during locomotion. These visualizations suggested that this collective neural activity resided in different states in a high-dimensional space depending on the animal's locomotor behavior. However, it is difficult to compare changes in neural activity during locomotion across animals as differences in the dimensionality for each animal depend on analysis method. We instead turned to a measure of statistical dispersion of firing patterns in M/T cells, entropy, that quantifies the diversity of states across ensembles when the animal is running versus when it is stationary. To do this, we binarized spike trains from subsampled ensembles of M/T cells into patterns of 1s and 0s and calculated the entropy of the activity when the animal was stationary versus when it was running (**Fig. 4A**). For 500 resamples of 8-unit subpopulations in a single animal, entropy (denoted-H) was greater when running as compared to when the animal was stationary ($H_{stationary}$ = 77.4$\pm$28 bits/sec, $H_{running}$ =85.7$\pm$35 bits/sec, $p < 0.05$, two-sided Wilcoxon signed-rank test, **Fig. 4B**). The increase in entropy was also significant across the all recording sessions in animals ($H_{stationary}$ = 82.7+11 bits/sec, $H_{running}$ = 91.8$\pm$13 bits/sec , $p < 0.005$, two-sided Wilcoxon signed-rank test, N = 6, **Fig. 4C** inset). Furthermore, the entropy was significantly larger with running over a range of subpopulation sizes from 2 to 25 neurons ($p < 0.005$ for all populations from 2-25 neurons, two-sided Wilcoxon signed-rank test with Bonferroni

correction, **Fig. 4C**). Additionally, the entropy was larger during locomotion across a variety of additional bin sizes (50 ms, 100 ms, data not shown), meaning the number of patterns of spontaneous activity when the animal was locomoting were larger.

We next wished to identify what features of the ensemble activity gave rise to the changes in the entropy, and what these might reveal about how the structure of population activity is shaped by behavior. To do this, we constructed maximum-entropy models of M/T cell activity, which incorporate as few *a priori* assumptions about population interactions as possible (Chockanathan et al. 2020; Meshulam et al. 2017; Schneidman et al. 2006). These models contain a local field term ($\mathbf{h_i}$) for each neuron as well as a coupling term ($\mathbf{J_{ij}}$) for each pair of neurons. The local field term $\mathbf{h_i}$, is a measure of how likely the cell is to spike, the more negative, the more silent the firing of the neuron. The $\mathbf{J_{ij}}$ terms captured the interactions, the functional coupling across all pairs of cells. Both terms were calculated directly from the population activity when the animal was stationary versus when it was running (**Fig. 5A**), effectively identifying how the baseline firing and pair-wise interactions between neurons were altered when the animal ran. Using these terms for pairs of neurons, we then predicted the frequency of patterns across the population that should occur based on pair-wise interactions and compared the predicted patterns to those observed in the data (**Fig. 5B** representative 8-unit subsample from a single animal). The closer to the unity line (black), the better the model was at predicting patterns of activity. In this example, predictions of patterns from the model during running were worse than those during stationary epochs (**Fig. 5C**). The difference in prediction between the model and the data was quantified using the Kullbeck-Liebler divergence (KLD). For example, when comparing the fits at the

271 group level for an 11-unit population, the KLD was increased for running epochs as
272 compared to stationary epochs, indicating that the fit was worse when the animals ran
273 ($KLD_{stationary} = 0.0012 \pm 0.0008$, $KLD_{running} = 0.0040 \pm 0.0015$, $p < 0.05$, two-sided
274 Wilcoxon signed-rank test, N = 6, **Fig. 5D** inset). Across a range of subpopulation sizes
275 (3 to 19 units), the pair-wise maximum entropy model was worse at predicting the global
276 patterns of activity when the animal was running as compared to when it was stationary
277 ($p < 0.05$, two-sided Wilcoxon signed-rank test with Bonferroni correction, **Fig. 5D**).
278 To understand what the maximum entropy models revealed about ensemble
279 activity in the bulb, we examined the mathematical structure of the maximum entropy
280 distribution, the $\mathbf{h_i}$ and $\mathbf{J_{ij}}$ terms. The local field term $\mathbf{h_i}$, was always significantly higher
281 during running as compared to when the animal was stationary (for 11-unit
282 subpopulation: $\mathbf{h_{i,running}} = -5.20 \pm 1.67$, $\mathbf{h_{i,stationary}} = -5.42 \pm 1.81$, $p < 0.005$, two-sided
283 Wilcoxon signed-rank test, **Fig. 5E**, right) across subpopulations ranging in size from 3
284 to 19 neurons ($p < 10^{-6}$, two-sided Wilcoxon signed-rank test with Bonferroni correction,
285 **Fig. 5F**), consistent with the mean increase in firing rates observed when the animal ran
286 (**Fig. 2D**). Interestingly, the distributions of the $\mathbf{J_{ij}}$ terms which captured the interactions
287 between neurons were significantly decreased during running (for 11-unit
288 subpopulation: $\mathbf{J_{ij,stationary}} = 0.41 \pm 1.15$; $\mathbf{J_{ij,running}} = -0.08 \pm 0.95$, $p < 0.005$, two-sided
289 Wilcoxon signed-rank test, **Fig. 5G**, right)**.** Furthermore, while the mean $\mathbf{J_{ij}}$ term was
290 positive during stationary epochs across an array of subpopulation sizes (3-19
291 neurons), the $\mathbf{J_{ij}}$ terms were slightly negative during running epochs, ($p < 10^{-6}$ for all
292 population sizes, two-sided Wilcoxon signed-rank test with Bonferroni correction, **Fig.**
293 **5H**). This result, combined with our entropy findings (**Fig. 4A**), provides insight into the

294 poorer fit of the model during running epochs. While the increased entropy showed that
295 population patterns in the MOB became more diverse with running (**Fig. 4**), the
296 diminished $\mathbf{J_{ij}}$ interaction terms during running meant the pair-wise maximum entropy
297 models were comparatively insufficient to capture the increased complexity of ensemble
298 activity.

299 Previous work has suggested that the interaction term $\mathbf{J_{ij}}$ is related to pairwise
300 correlations between neurons (Schneidman et al. 2006). To explore this, we calculated
301 the pair-wise correlation for every pair of units in each animal during stationary and
302 running epochs (**Fig. 6A**). While the $\mathbf{J_{ij}}$ terms were estimated and then iteratively
303 updated to improve their fit (see *Materials and Methods)* (Maoz and Schneidman 2017),
304 the pairwise correlation was directly calculated from continuous firing rate time-series.
305 They thus represented two complementary methods for assessing pairwise interactions.
306 We found that the pairwise correlations during running were smaller than that during
307 stationary epochs (**Fig. 6B**,**C**), consistent with the finding of $\mathbf{J_{ij}}$ terms based on behavior
308 (**Fig. 5G**,**H**), demonstrating that during locomotion, not only the firing rates but the
309 interactions between neurons are affected.
310

311 **Discussion**

312 Here we found that mitral/tufted cell population activity in the main olfactory bulb
313 of the mouse changed during the animal's locomotion. In addition to increases in firing
314 rates of individual neurons, the entropy of population activity was increased when the
315 animal ran, resulting in an increase in the dimensionality of the ensemble activity. A
316 second order maximum entropy model fit to the population activity revealed that weak-

317 pairwise interactions could explain the global structure of the firing when the animal was
318 stationary, but the explanatory power of these pairwise interactions diminished when the
319 animal ran. We therefore suggest that running is associated with higher-order
320 interactions between M/T cells.

321 What do these changes in neuronal population activity signify in terms of
322 olfactory function? Without recordings of population responses to arrays of odors while
323 the animal is running versus when it remains stationary, the information content of the
324 neuronal ensemble cannot be extrapolated from the entropy. These information
325 estimates depend heavily on how the stimulus domain is partitioned (how different are
326 the odors, odor classes, concentrations, etc.) as well as the sampling (number of stimuli
327 presented, number of trials, etc.) (Hallem and Carlson 2006; Meister and Bonhoeffer
328 2001; Rubin and Katz 1999; Saito et al. 2009; Soucy et al. 2009), questions we leave
329 for future work. We instead focus on the question of how locomotor behavior reshapes
330 the structure of spontaneous activity in the olfactory bulb. Previous work has shown
331 that running is associated with increased whisking, sniffing, and spontaneous firing
332 rates in M/T cells. Interestingly, while we find this to be true for a number of M/T cells,
333 we also find a number of neurons whose firing rate reduces with running. Additionally,
334 while we were not able to measure sniffing in these experiments, recent studies
335 demonstrate the sniffing in head fixed animals may be different than freely behaving
336 animals (Nguyen Chi et al. 2016). While sniffing, whisking, neural circuits could give
337 rise to changes in both single cell and population M/T cell activity (Carey and
338 Wachowiak 2011; Kleinfeld et al. 2014; Moore et al. 2013; Wachowiak 2011), here we

focus on *how* these behaviors during running could influence neural population activity, and what this might mean for general principles of encoding.

First, studies in visual cortex (MacLean et al. 2005; Niell and Stryker 2010), auditory cortex (Bender et al. 2016; Luczak et al. 2009), and the olfactory bulb (Stakic et al. 2011; Thompson et al. 2018) suggest that patterns of spontaneous activity recapitulate patterns of activity in response to sensory stimuli (Carrillo-Reid et al. 2019; MacLean et al. 2005; Tsodyks et al. 1999), effectively outlining the realm of possible patterns that *can* occur in response to inputs (Luczak et al. 2009; Thompson et al. 2018). As entropy increases and pair-wise correlations decrease during locomotion, our results suggest that the realm of possible patterns of activity when the animal was running are larger. Consequently, if spontaneous activity defines a manifold on which responses to odors reside (Chen and Padmanabhan 2020; Thompson et al. 2018), then our study shows that the size of that manifold is larger when the animal runs. Recent evidence suggests that spontaneous activity in the olfactory cortex (piriform cortex) is driven by the firing of neurons in the bulb (Tantirigama et al. 2017). Changes in the structure of spontaneous activity in the bulb during locomotion may therefore dynamically gate the range of olfactory coding in the piriform cortex. Furthermore, as pair-wise correlations are better at describing the patterns that occur when the animal is stationary as compared to when it is running, our work suggests that the space in which olfactory responses reside during locomotion may be more complex, and defined by higher order interactions among neurons (Ohiorhenuan et al. 2010; Schneidman et al. 2011; Tkačik et al. 2014).

How do these functional differences arise? Maximum entropy models can be thought of as a way to generate null hypotheses about the functional connectivity within neural circuits (Schneidman 2016). In the retina for instance, pair-wise maximum entropy models are sufficient to account for the joint activity of ensembles of neurons (Schneidman et al. 2006; Shlens et al. 2006), a statistical description of observed patterns that arise from the anatomical constraints of the circuits (Pillow et al. 2008; Shlens et al. 2006). By contrast, these same pair-wise interaction models fail to account for the joint activity of populations as small as 5 neurons in the primary visual cortex (Ohiorhenuan et al. 2010) suggesting that higher order structure (3rd, 4th order), possibly arising from interactions with local inhibitory interneurons, may govern the structure of neuronal population activity. In the bulb, the dense interconnectedness between M/T cells and granule cells (Kapoor and Urban 2006; Willhite et al. 2006) suggests that the earliest stages of olfactory processing may be more like cortex than retina. Importantly, although organized in some columnar structure (Willhite et al. 2006), the M/T cell interactions with inhibitory granule cells can extend across large spatial scales throughout the bulb (Burton 2017; Gilra and Bhalla 2015; Migliore et al. 2010), possibly more akin to long range connections in cortical circuits (Ruthazer and Stryker 1996). Additionally, granule cells receive centrifugal inputs from a number of regions including the anterior olfactory nucleus (AON), the piriform cortex, the horizontal diagonal band, and the raphe nucleus (Petzold et al. 2009; Price and Powell 1970; Rothermel and Wachowiak 2014; Shipley and Adamek 1984). Among these, monosynaptic projections from both the ventral CA1 (vCA1) region of the hippocampus and the entorhinal cortex (Davis and Macrides 1981; Padmanabhan et al.

2018) may be candidate circuits relaying locomotion information to the bulb, altering the activity of M/T cells via the local inhibitory interneuron population. We caution that how locomotion is operationalized in this work is experimentally constrained, as animals are head-fixed and run on a cylinder, with behavior delineated into epochs of stationary versus running. Nonetheless, these experimental distinctions between “stationary” and “running” may correspond to ethologically different behavioral modes. Locomotion for instance, is necessarily engaged in odor navigation and tracking (Gire et al. 2016; Khan et al. 2012), while animals are often stationary when sniffing a single object in service of odor discrimination or odor identification (Kepecs et al. 2007; Rinberg et al. 2006b; Uchida and Mainen 2003). These different behavioral modes may require either different underlying coding strategies or may include information about behavior itself in the code relayed by M/T cells. Our results suggest that the structure of spontaneous activity in the bulb is highly flexible to support these different modes, operating within a dynamic high-dimensional space shaped by the animal’s behavior (Tsuno and Mori 2009).

Disclosures

No conflicts of interest, financial or otherwise, are declared by the author(s).

Authors Contributions

K.P. conceived and supervised the project. K.P. and U.C. performed the analysis, made the figures, and wrote the manuscript. E.J.W.C. and K.P. performed the experiments. R.C.G, S.W. and E.L. assisted with analyses. All authors approved the final version of the manuscript.

Acknowledgements

KP was supported by NSF CAREER (1749772), NIMH (R01MH11392), the Schmitt Foundation, and the Cystinosis Research Foundation. RCG was supported by NINDS (U19NS112953) and NIDCD (R01DC018455).

References

Abraham NM, **Egger V**, **Shimshek DR**, **Renden R**, **Fukunaga I**, **Sprengel R**, **Seeburg PH**, **Klugmann M**, **Margrie TW**, **Schaefer AT**, **Kuner T**. Synaptic inhibition in the olfactory bulb accelerates odor discrimination in mice. *Neuron* 65: 399–411, 2010.

Bender DA, **Ni R**, **Barbour DL**. Spontaneous activity is correlated with coding density in primary auditory cortex. *J Neurophysiol* , 2016. doi:10.1152/jn.00474.2016.

Burton SD. Inhibitory circuits of the mammalian main olfactory bulb. *J Neurophysiol* 118: 2034–2051, 2017.

Carey RM, **Wachowiak M**. Effect of sniffing on the temporal structure of mitral/tufted cell output from the olfactory bulb. *The Journal of neuroscience : the official journal of the Society for Neuroscience* 31: 10615–26, 2011.

Carrillo-Reid L, **Han S**, **Yang W**, **Akrouh A**, **Yuste R**. Controlling Visually Guided Behavior by Holographic Recalling of Cortical Ensembles. *Cell* 178: 447-457.e5, 2019.

Chen Z, **Padmanabhan K**. Top-down Control of Inhibitory Granule Cells in the Main Olfactory Bulb Reshapes Neural Dynamics Giving Rise to a Diversity of Computations. *Front Comput Neurosci* 14, 2020.

Chockanathan U, **Warner EJ**, **Turpin L**, **O'Banion MK**, **Padmanabhan K**. Altered dorsal CA1 neuronal population coding in the APP/PS1 mouse model of Alzheimer's disease. *Scientific Reports* 10: 1–12, 2020.

Constantinople CM, **Bruno RM**. Effects and mechanisms of wakefulness on local cortical networks. *Neuron* 69: 1061–1068, 2011.

Dadarlat MC, **Stryker MP**. Locomotion Enhances Neural Encoding of Visual Stimuli in Mouse V1. *The Journal of neuroscience : the official journal of the Society for Neuroscience* 37: 3764–3775, 2017.

Davis BJ, **Macrides F**. The organization of centrifugal projections from the anterior olfactory nucleus, ventral hippocampal rudiment, and piriform cortex to the main olfactory bulb in the hamster: an autoradiographic study. *The Journal of comparative neurology* 203: 475–93, 1981.

Dhawale AK, **Hagiwara A**, **Bhalla US**, **Murthy VN**, **Albeanu DF**. Non-redundant odor coding by sister mitral cells revealed by light addressable glomeruli in the mouse. *Nature neuroscience* 13: 1404–12, 2010.

447 **Dipoppa M**, **Ranson A**, **Krumin M**, **Pachitariu M**, **Carandini M**, **Harris KD**. Vision and
448 Locomotion Shape the Interactions between Neuron Types in Mouse Visual Cortex. *Neuron* 98:
449 602-615.e8, 2018.

450 **Doucette W**, **Gire DH**, **Whitesell J**, **Carmean V**, **Lucero MT**, **Restrepo D**. Associative cortex
451 features in the first olfactory brain relay station. *Neuron* 69: 1176–1187, 2011.

452 **Doucette W**, **Restrepo D**. Profound context-dependent plasticity of mitral cell responses in
453 olfactory bulb. *PLoS biology* 6: e258, 2008.

454 **Du J**, **Blanche TJ**, **Harrison RR**, **Lester HA**, **Masmanidis SC**. Multiplexed, High Density
455 Electrophysiology with Nanofabricated Neural Probes. *PLOS ONE* 6: e26204, 2011.

456 **Erisken S**, **Vaiceliunaite A**, **Jurjut O**, **Fiorini M**, **Katzner S**, **Busse L**. Effects of Locomotion Extend
457 throughout the Mouse Early Visual System. *Current Biology* 24: 2899–2907, 2014.

458 **Gerkin RC**, **Tripathy SJ**, **Urban NN**. Origins of correlated spiking in the mammalian olfactory
459 bulb. *Proceedings of the National Academy of Sciences of the United States of America* 110:
460 17083–8, 2013.

461 **Gilra A**, **Bhalla US**. Bulbar microcircuit model predicts connectivity and roles of interneurons in
462 odor coding. *PLoS ONE* 10: e0098045, 2015.

463 **Gire DH**, **Kapoor V**, **Arrighi-Allisan A**, **Seminara A**, **Murthy VN**. Mice Develop Efficient Strategies
464 for Foraging and Navigation Using Complex Natural Stimuli. *Curr Biol* 26: 1261–1273, 2016.

465 **Gourevitch B**, **Kay LM**, **Martin C**. Directional Coupling From the Olfactory Bulb to the
466 Hippocampus During a Go/No-Go Odor Discrimination Task. *Journal of Neurophysiology* 103:
467 2633–2641, 2010.

468 **Hallem EA**, **Carlson JR**. Coding of Odors by a Receptor Repertoire. *Cell* 125: 143–160, 2006.

469 **Kapoor V**, **Urban NN**. Glomerulus-specific, long-latency activity in the olfactory bulb granule cell
470 network. *The Journal of neuroscience : the official journal of the Society for Neuroscience* 26:
471 11709–19, 2006.

472 **Kay LM**, **Laurent G**. Odor- and context-dependent modulation of mitral cell activity in behaving
473 rats. *Nature neuroscience* 2: 1003–9, 1999.

474 **Kepecs A**, **Uchida N**, **Mainen ZF**. Rapid and precise control of sniffing during olfactory
475 discrimination in rats. *J Neurophysiol* 98: 205–213, 2007.

476 **Khan AG**, **Sarangi M**, **Bhalla US**. Rats track odour trails accurately using a multi-layered strategy
477 with near-optimal sampling. *Nature communications* 3: 703, 2012.

Kleinfeld D, **Deschênes M**, **Wang F**, **Moore JD**. More than a rhythm of life: breathing as a binder of orofacial sensation. *Nature Neuroscience* 17: 647–651, 2014.

Kobayakawa K, **Kobayakawa R**, **Matsumoto H**, **Oka Y**, **Imai T**, **Ikawa M**, **Okabe M**, **Ikeda T**, **Itohara S**, **Kikusui T**, **Mori K**, **Sakano H**. Innate versus learned odour processing in the mouse olfactory bulb. *Nature* 450: 503–8, 2007.

Lewicki M. A review of methods for spike sorting: the detection and classification of neural action potentials. *Network: Computation in Neural Systems* 9: R53–R78, 1998.

Luczak A, **Barthó P**, **Harris KD** Spontaneous events outline the realm of possible sensory responses in neocortical populations. *Neuron* 62: 413–25, 2009.

MacLean JN, **Watson BO**, **Aaron GB**, **Yuste R**. Internal dynamics determine the cortical response to thalamic stimulation. *Neuron* 48: 811–823, 2005.

Maoz O, **Schneidman E**. maxent_toolbox: Maximum entropy toolbox for MATLAB, version 1.0.2. 2017.

Meister M, **Bonhoeffer T**. Tuning and topography in an odor map on the rat olfactory bulb. *The Journal of neuroscience : the official journal of the Society for Neuroscience* 21: 1351–60, 2001.

Meshulam L, **Gauthier JL**, **Brody CD**, **Tank DW**, **Bialek W**. Collective Behavior of Place and Non-place Neurons in the Hippocampal Network. *Neuron* 96: 1178-1191.e4, 2017.

Migliore M, **Hines ML**, **McTavish TS**, **Shepherd GM**. Functional roles of distributed synaptic clusters in the mitral-granule cell network of the olfactory bulb. *Front Integr Neurosci* 4: 122, 2010.

Moore JD, **Deschênes M**, **Furuta T**, **Huber D**, **Smear MC**, **Demers M**, **Kleinfeld D**. Hierarchy of orofacial rhythms revealed through whisking and breathing. *Nature* 497: 205–210, 2013.

Murthy VN. Olfactory maps in the brain. *Annual review of neuroscience* 34: 233–58, 2011.

Nguyen Chi V, **Müller C**, **Wolfenstetter T**, **Yanovsky Y**, **Draguhn A**, **Tort ABL**, **Brankačk J**. Hippocampal Respiration-Driven Rhythm Distinct from Theta Oscillations in Awake Mice. *J Neurosci* 36: 162–177, 2016.

Niell CM, **Stryker MP**. Modulation of visual responses by behavioral state in mouse visual cortex. *Neuron* 65: 472–479, 2010.

Ohiorhenuan IE, **Mechler F**, **Purpura KP**, **Schmid AM**, **Hu Q**, **Victor JD**. Sparse coding and high-order correlations in fine-scale cortical networks. *Nature* 466: 617–621, 2010.

Padmanabhan K, **Osakada F**, **Tarabrina A**, **Kizer E**, **Callaway EM**, **Gage FH**, **Sejnowski TJ**. Diverse Representations of Olfactory Information in Centrifugal Feedback Projections. *The Journal of neuroscience : the official journal of the Society for Neuroscience* 36: 7535–45, 2016.

Padmanabhan K, **Osakada F**, **Tarabrina A**, **Kizer E**, **Callaway EM**, **Gage FH**, **Sejnowski TJ**. Centrifugal Inputs to the Main Olfactory Bulb Revealed Through Whole Brain Circuit-Mapping. *Frontiers in neuroanatomy* 12: 115, 2018.

Petzold GC, **Hagiwara A**, **Murthy VN**. Serotonergic modulation of odor input to the mammalian olfactory bulb. *Nature neuroscience* 12: 784–91, 2009.

Pillow JW, **Shlens J**, **Paninski L**, **Sher A**, **Litke AM**, **Chichilnisky EJ**, **Simoncelli EP**. Spatio-temporal correlations and visual signalling in a complete neuronal population. *Nature* 454: 995–9, 2008.

Price JL, **Powell TP**. An experimental study of the origin and the course of the centrifugal fibres to the olfactory bulb in the rat. *Journal of anatomy* 107: 215–37, 1970.

Price JL, **Powell TP**. Certain observations on the olfactory pathway. *Journal of anatomy* 110: 105–26, 1971.

Pryluk R, **Kfir Y**, **Pryluk R**, **Kfir Y**, **Gelbard-sagiv H**, **Fried I**, **Paz R**. A Tradeoff in the Neural Code across Regions and Species. *Cell* 176: 597-609.e18, 2019.

Rinberg D, **Koulakov A**, **Gelperin A**. Sparse odor coding in awake behaving mice. *The Journal of neuroscience : the official journal of the Society for Neuroscience* 26: 8857–65, 2006a.

Rinberg D, **Koulakov A**, **Gelperin A**. Speed-accuracy tradeoff in olfaction. *Neuron* 51: 351–8, 2006b.

Rothermel M, **Wachowiak M**. Functional imaging of cortical feedback projections to the olfactory bulb. *Frontiers in Neural Circuits* 8: 73, 2014.

Rubin BD, **Katz LC**. Optical imaging of odorant representations in the mammalian olfactory bulb. *Neuron* 23: 499–511, 1999.

Ruthazer ES, **Stryker MP**. The role of activity in the development of long-range horizontal connections in area 17 of the ferret. *The Journal of neuroscience : the official journal of the Society for Neuroscience* 16: 7253–69, 1996.

de Ruyter van Steveninck RR, **Lewen GD**, **Strong SP**, **Koberle R**, **Bialek W**, **Steveninck RRDR Van**, **Lewen GD**, **Strong SP**, **Koberle R**, **Bialek W**. Reproducibility and Variability in Neural Spike Trains. *Science (New York, NY)* 275: 1805–1808, 1997.

Saito H, **Chi Q**, **Zhuang H**, **Matsunami H**, **Mainland JD**. Odor coding by a Mammalian receptor repertoire. *Science signaling* 2: ra9, 2009.

Schneidman E. Towards the design principles of neural population codes. *Curr Opin Neurobiol* 37: 133–140, 2016.

Schneidman E, **Berry MJ**, **Segev R**, **Bialek W**. Weak pairwise correlations imply strongly correlated network states in a neural population. *Nature* 440: 1007–1012, 2006.

Schneidman E, **Puchalla JL**, **Segev R**, **Harris RA**, **Bialek W**, **Berry MJ**. Synergy from silence in a combinatorial neural code. *J Neurosci* 31: 15732–15741, 2011.

Shipley MT, **Adamek GD**. The connections of the mouse olfactory bulb: a stu... [Brain Res Bull. 1984] - PubMed result. *Brain research bulletin* 12: 669–88, 1984.

Shlens J, **Field GD**, **Gauthier JL**, **Grivich MI**, **Petrusca D**, **Sher A**, **Litke AM**, **Chichilnisky EJ**. The structure of multi-neuron firing patterns in primate retina. *J Neurosci* 26: 8254–8266, 2006.

Smear M, **Resulaj A**, **Zhang J**, **Bozza T**, **Rinberg D**. Multiple perceptible signals from a single olfactory glomerulus. *Nature neuroscience* 16: 1687–91, 2013.

Soucy ER, **Albeanu DF**, **Fantana AL**, **Murthy VN**, **Meister M**. Precision and diversity in an odor map on the olfactory bulb. *Nature neuroscience* 12: 210–20, 2009.

Stakic J, **Suchanek JM**, **Ziegler GP**, **Griff ER**. The source of spontaneous activity in the main olfactory bulb of the rat. *PLoS ONE* 6: e23990, 2011.

Stringer C, **Pachitariu M**, **Steinmetz N**, **Reddy CB**, **Carandini M**, **Harris KD**. Spontaneous behaviors drive multidimensional, brainwide activity. *Science* 364, 2019.

Tantirigama MLS, **Huang HH-Y**, **Bekkers JM**. Spontaneous activity in the piriform cortex extends the dynamic range of cortical odor coding. *Proc Natl Acad Sci USA* 114: 2407–2412, 2017.

Thompson GJ, **Sanganahalli BG**, **Baker KL**, **Herman P**, **Shepherd GM**, **Verhagen JV**, **Hyder F**. Spontaneous activity forms a foundation for odor-evoked activation maps in the rat olfactory bulb. *Neuroimage* 172: 586–596, 2018.

Tkačik G, **Marre O**, **Amodei D**, **Schneidman E**, **Bialek W**, **Berry MJ**. Searching for collective behavior in a large network of sensory neurons. *PLoS Comput Biol* 10: e1003408, 2014.

Tsodyks M, **Kenet T**, **Grinvald A**, **Arieli A**. Linking spontaneous activity of single cortical neurons and the underlying functional architecture. *Science (New York, NY)* 286: 1943–6, 1999.

Tsuno Y, **Kashiwadani H**, **Mori K**. Behavioral state regulation of dendrodendritic synaptic inhibition in the olfactory bulb. *J Neurosci* 28: 9227–9238, 2008.

Tsuno Y, **Mori K**. Behavioral state-dependent changes in the information processing mode in the olfactory system. *Commun Integr Biol* 2: 362–364, 2009.

572 **Uchida N**, **Mainen ZF**. Speed and accuracy of olfactory discrimination in the rat. *Nat Neurosci* 6:
573 1224–1229, 2003.

574 **Verhagen JV**, **Wesson DW**, **Netoff TI**, **White JA**, **Wachowiak M**. Sniffing controls an adaptive
575 filter of sensory input to the olfactory bulb. *Nature neuroscience* 10: 631–9, 2007.

576 **Vinck M**, **Batista-Brito R**, **Knoblich U**, **Cardin JA**. Arousal and Locomotion Make Distinct
577 Contributions to Cortical Activity Patterns and Visual Encoding. *Neuron* 86: 740–754, 2015.

578 **Wachowiak M**. All in a sniff: olfaction as a model for active sensing. *Neuron* 71: 962–73, 2011.

579 **Willhite DC**, **Nguyen KT**, **Masurkar AV**, **Greer CA**, **Shepherd GM**, **Chen WR**. Viral tracing
580 identifies distributed columnar organization in the olfactory bulb. *Proceedings of the National*
581 *Academy of Sciences of the United States of America* 103: 12592–7, 2006.

582 **Wilson RI**, **Mainen ZF**. EARLY EVENTS IN OLFACTORY PROCESSING [Online].
583 2006http://www.annualreviews.org/doi/abs/10.1146/annurev.neuro.29.051605.112950?url_v
584 er=Z39.88-
585 2003&rfr_dat=cr_pub%253Dpubmed&rfr_id=ori%253Arid%253Acrossref.org&journalCode=neu
586 ro.

587

588

589

590

591

592

593

594

595

596

597

598

599

600

601

602

603

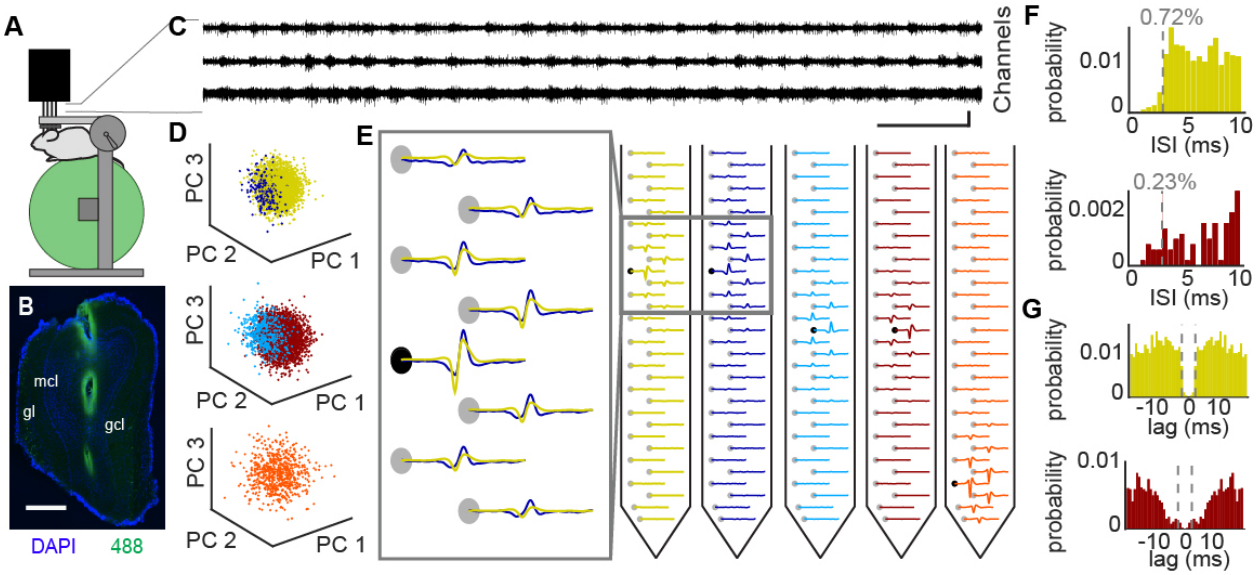

Figure 1: Electrophysiological monitoring of large ensembles of mitral/tufted cells in a head-fixed animal on a run wheel. (A) Schematic of recording population activity from Mitral/tufted cells in the main olfactory bulb of awake mice affixed to a run-wheel. (B) Coronal section of MOB showing recording location (labeled by cholera toxin B subunit conjugated to Alexa 488). Scale bar = 100 μm. (C) Bandpass (500-3500 Hz) voltage trace from 3 channels of 128 channels show spiking activity across multiple contacts. (D) PCA projections of spike waveform clusters used for identifying single units. Each color represents a waveform from E, each point is a single spike. (E, left) Spike waveforms of two units across 8 channels from a single 32 channel shank. (E, right) Waveforms across all 32 channels for 5 units show that spiking activity from a single cell can be found across 8-12 contacts. (F) Inter-spike interval histogram for two units in D and E. (F) Auto-correlation of spike counts from two units in D and E.

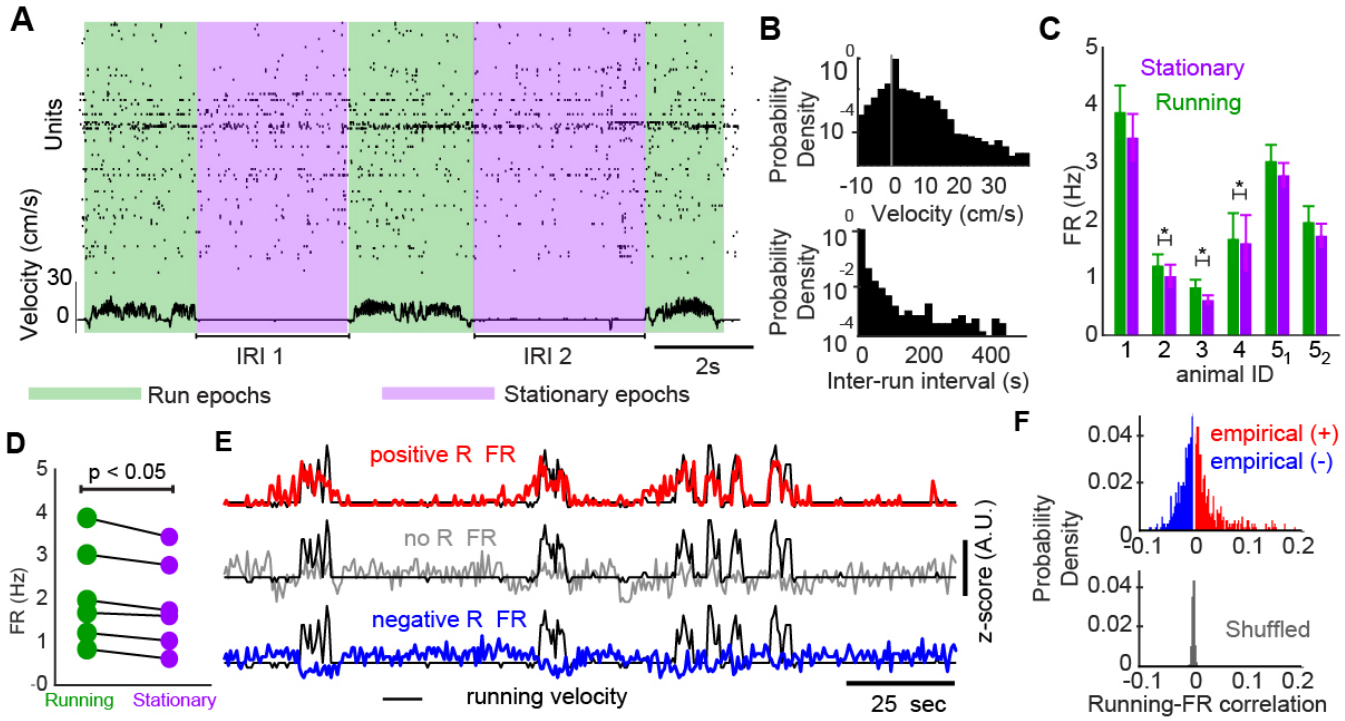

Figure 2: M/T cell firing was modulated by locomotion. (A) Example trace of ensemble of recorded units while the animal was running (green) versus when it was stationary (purple). (B, top) Histogram of run velocity across all animals. (B, bottom) Histogram of inter-run intervals. (C) Mean firing rate across units for 6 recording sites across 5 animals. Firing rates were significantly higher in 3 animals when the animal ran. (D) Firing rates were significantly higher on average during running across all recording sites from all animals (N = 6). (E) Example traces of unit firing rate and running velocity for a correlated unit (red), uncorrelated unit (gray), and negatively correlated unit (blue). (F) Histogram of correlations between unit firing rate and run velocity (top, positive correlated units = red, negatively correlated units = blue, bottom, shuffled data = gray).

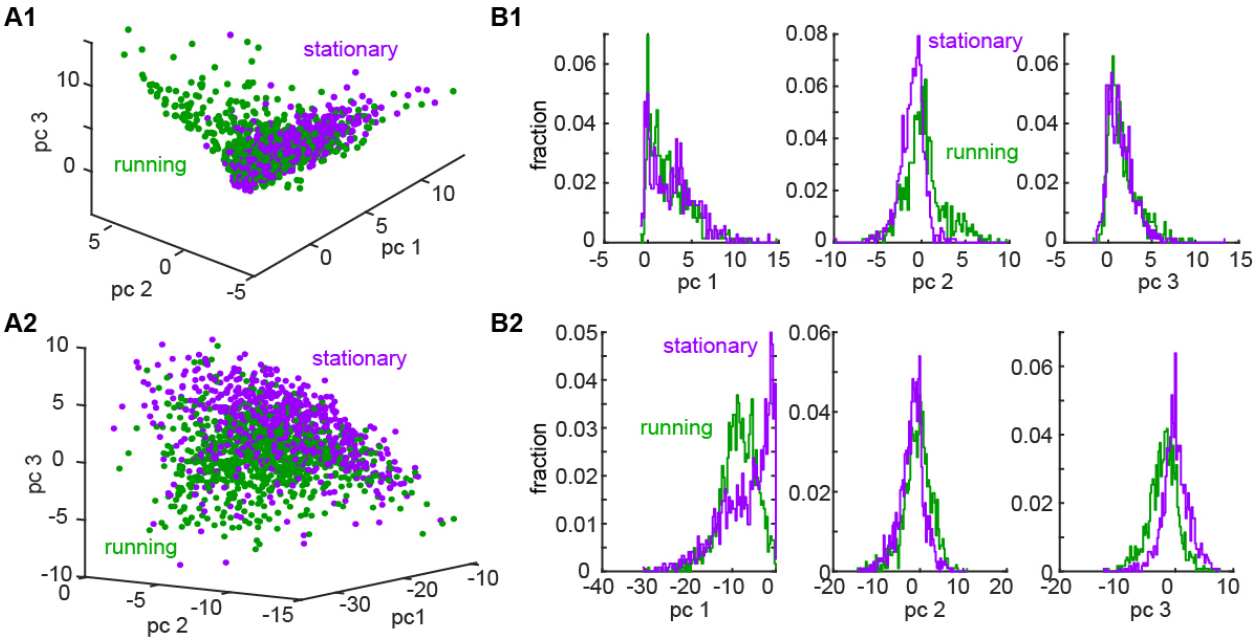

Figure 3: Ensemble activity was differentially distributed in a state space during running vs stationary epochs. (A) Two representative examples of ensemble activity from > 100 simultaneously recorded units projected onto a low dimensional space when the animal was running (green) versus when it was stationary (purple). Each dot corresponds to a single time. (B) Histograms of activity during running versus when the animals were stationary in each of the three dimensions in A.

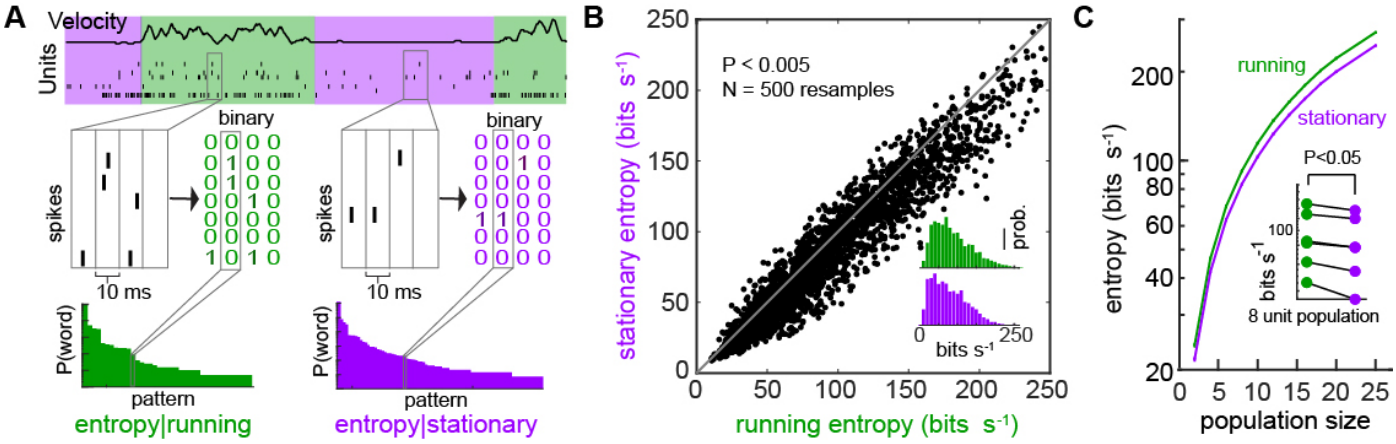

Figure 4: Entropy was greater when animals were running as compared to when they were stationary. (A) Schematic describing how ensemble activity was converted into binary patterns. Spikes were binned in 10 ms windows and converted to patterns of 1s and 0s. (B) Entropy for 500 subsamples of an 8 neuron population in a single animal during running versus stationary epochs. (B, insert) Histogram of entropy for running versus stationary epochs. (C) Entropy for different subpopulations sizes from 2 to 25 units (500 samples/animal/subpopulation size) shows that entropy was significantly higher when the animal was running as compared to when it was stationary. (C, insert) Mean entropy was lower when stationary as compared to running at the animal level.

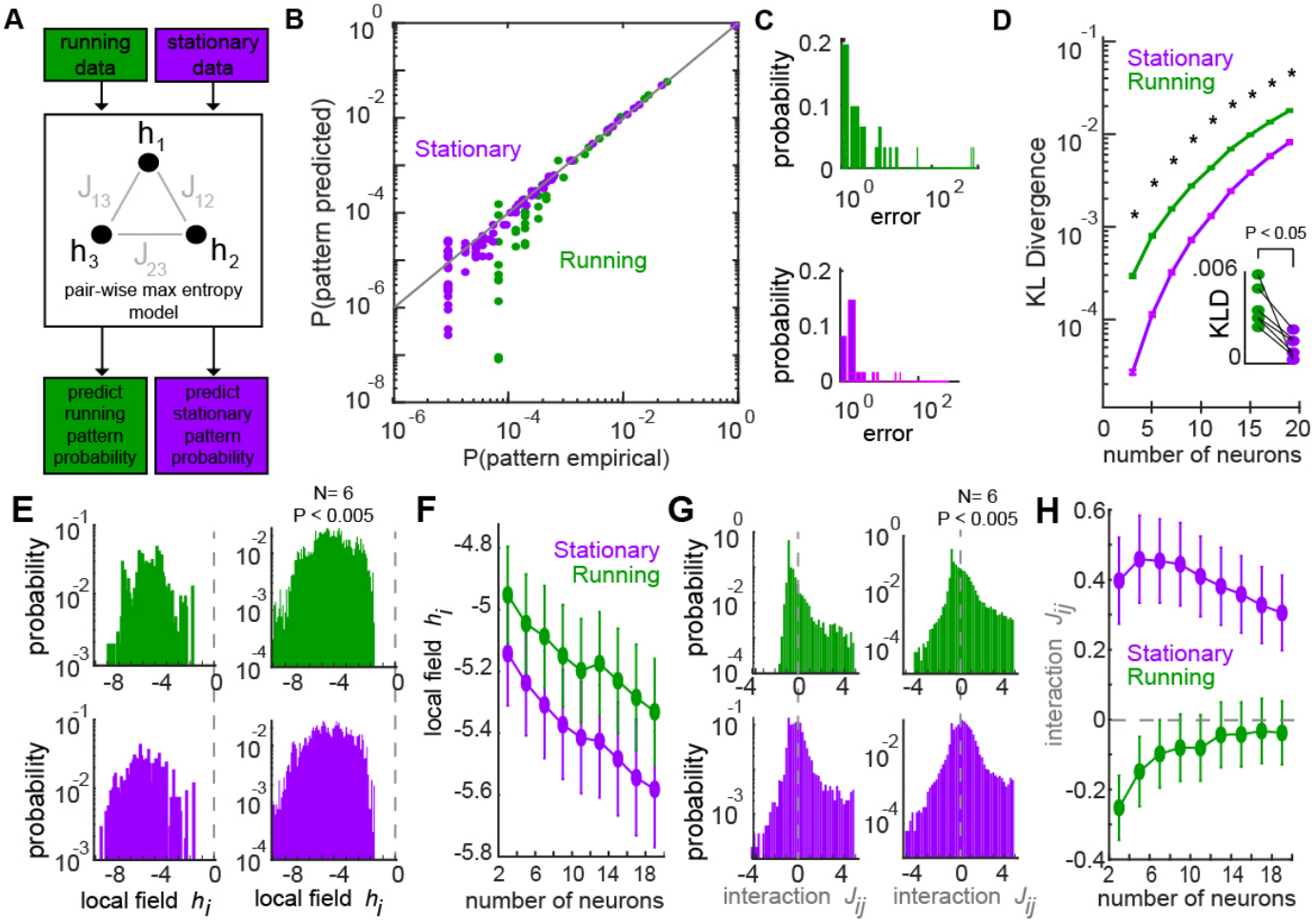

Figure 5: Pair-wise maximum entropy models were better at fitting M/T cell ensemble activity when the animal was stationary as compared to when it was running. (A) Schematic of method for calculating pair-wise maximum entropy models. (B) For an example 8-unit population, the rate occurrence of each firing pattern from the pair-wise maximum entropy model was plotted against the observed data for running (green) and stationary (purple) epochs. (C) Histograms of prediction error of rate of occurrence of the firing patterns in B showed that error was higher when the animal was running. (D) KL divergence, which measures the goodness of pair-wise maximum entropy model prediction for different subpopulations sizes from 3 to 19 units during running versus stationary epochs. (D, insert) Mean KLD for each recording session during running

versus stationary epochs. (E, left) Histogram of local field term of pair-wise maximum entropy model from a single animal across multiple resamples of an 8 unit subpopulation. (E, right) Histogram of local field term of pair-wise maximum entropy model from all recording sessions. (F) Mean local field term for different subpopulation sizes. (G, left) Histogram of interaction terms of pair-wise maximum entropy model from a single animal across multiple resamples of a 8 unit subpopulation. (G, right) Histogram of local field term of pair-wise maximum entropy model from all recording sessions. (H) Mean interaction term for different subpopulation sizes.

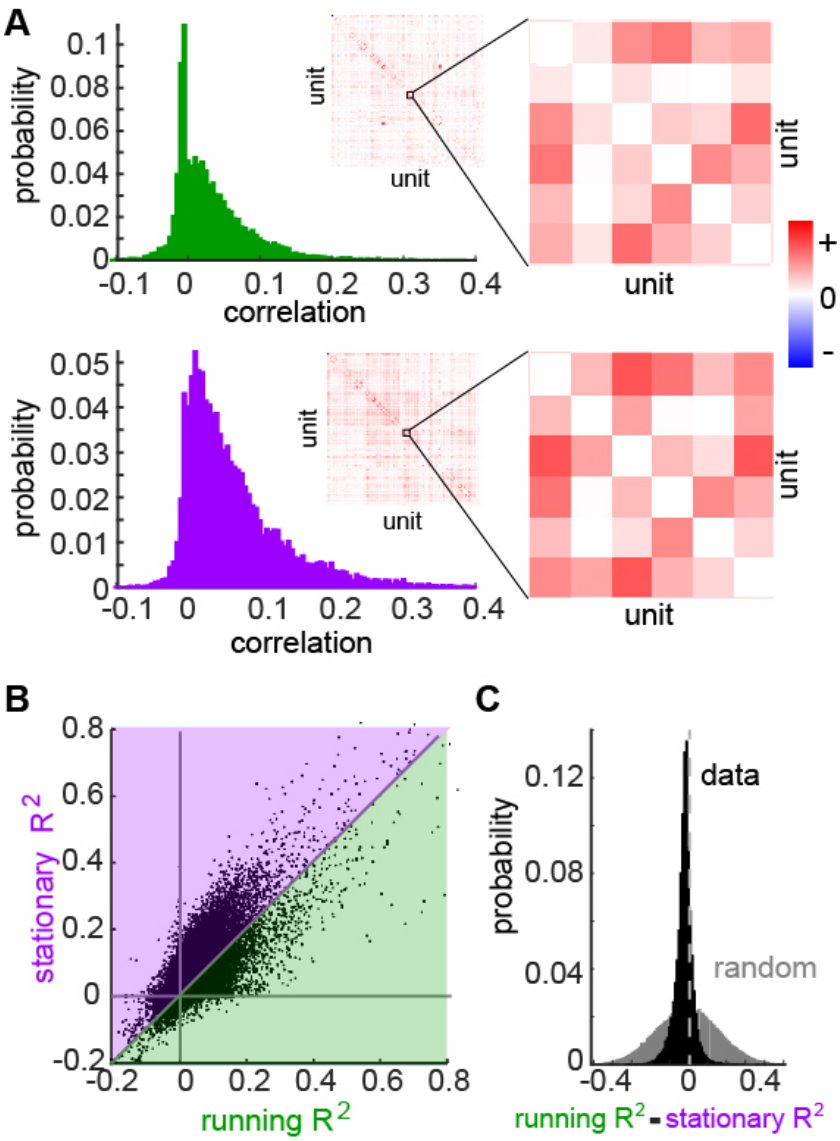

Figure 6: M/T cell pair-wise correlations were lower when animal was running. (A) Histogram of M/T cell pair-wise correlations for a single animal when the animal was running (top) versus when the animal was stationary (bottom). (A, insert) Correlation matrix for all pairs (positive correlations red, negative correlations =blue). (B) Correlated activity during running plotted against correlated activity when the animal was stationary. (C) Histogram of differences in correlation between when the animal was running versus stationary (black) as compared to shuffled data (gray).